J. Phys.: Condens. Matter **22** (2010) 315501 (7pp) doi:10.1088/0953-8984/22/31/315501

Hydrogen adsorption and carrier generation in $LaAlO_3$–$SrTiO_3$ heterointerfaces: a first-principles study

Won-joon Son[1], Eunae Cho[1], Jaichan Lee[2] and Seungwu Han[1]

[1] Department of Materials Science and Engineering, Seoul National University, Seoul 151-744, Korea
[2] School of Advanced Materials Science and Engineering, Sungkyunkwan University, Suwon 440-746, Korea

E-mail: hansw@snu.ac.kr

Received 1 March 2010, in final form 17 June 2010
Published 8 July 2010
Online at stacks.iop.org/JPhysCM/22/315501

Abstract

Using the first-principles method, we investigate the hydrogen adsorption on the polar AlO_2 surface of $LaAlO_3$–$SrTiO_3$ heterostructures with an n-type interface. It is found that the H atom is most stable when bound at the surface O atom. The adsorption energy for a given H density is lowered (i.e., stronger binding) with increasing $LaAlO_3$ thickness. The adsorbed H atom donates electrons to the conduction band of $SrTiO_3$, which results in the metallic conductivity of $SrTiO_3$. The charge transfer from H to $SrTiO_3$ significantly alters the electrostatic boundary condition and the Coulombic divergence inside $LaAlO_3$ completely disappears when one H atom is adsorbed every (2×1) surface unit cell. Our results also indicate that H_2 or H_2O molecules exothermically dissociate and adsorb on the surface when the $LaAlO_3$ layer is thicker than certain critical values, suggesting that the H adsorption may play a role in the conducting properties of $LaAlO_3$–$SrTiO_3$ heterostructures observed in experiment.

(Some figures in this article are in colour only in the electronic version)

1. Introduction

Because of the diverging nature of the electrostatic potential, a substantial reconstruction is required to stabilize the charged surface with a net dipole moment perpendicular to the surface direction [1, 2]. For example, the (001) polar surface of $LaAlO_3$ (LAO) exhibits a significant surface reconstruction and the delocalized fractional holes in the surface contribute to the charge compensation [3]. Similarly, in the heterointerface formed between LAO and $SrTiO_3$ (STO), the electrostatic instability of the LAO stack results in significant interfacial reconstructions [4]. To be specific, while atomic layers along the (001) direction in STO are neutral in their formal charges, those in LAO alternate with $+e$ and $-e$ for LaO and AlO_2 unit layers, respectively. This results in the Coulombic divergence in LAO unless half of an electron charge is accumulated or depleted at the interface. The carrier generation in the n-type LAO–STO interface with a sequence of $\cdots$–(AlO_2)–(LaO)–(TiO_2)–(SrO)–$\cdots$ has been regarded as a manifestation of the electronic reconstruction to satisfy this electrostatic boundary condition [4, 5]. This picture has been also supported by a series of first-principles calculations [6–11]. However, the microscopic details leading to the conductivity are still debated [12, 13]. For the clean interface without any defects, adsorbates, or interdiffusion, the first-principles study showed that electrons transfer from the LAO surface to the conduction bands of STO with a dependence on the LAO thickness similar to experiment [10]. However, it was also suggested that atomic interdiffusion at the interface [14] or the presence of oxygen vacancies in the LAO surface [15, 16] could account for the conductivity of the LAO–STO heterointerface.

It is well established that the polar surface can achieve neutrality by inviting foreign atoms such as hydrogen or hydroxyl groups [17]. In addition, due to the electron-donating nature of atomic hydrogen, the hydrogen adsorption on the oxide surface frequently increases the conductivity of the materials, which forms the basis of the hydrogen-sensing mechanism in several oxides [18, 19]. Motivated by this, in this work we study the H adsorption on the surface of LAO–STO heterostructures to investigate the possibility of

adsorption-induced metallicity of the heterointerface. We find that the H adsorption on the LAO surface can lead to metallicity in the STO substrate. It is also found that the adsorption energy decreases with the LAO thickness and the dissociative adsorption of H_2 or H_2O molecules can occur for thick LAO layers.

2. Computational methods and model systems

Throughout this work, we use first-principles methods using the VASP package [20]. The interaction between electrons and ions is described by the projector-augmented wave (PAW) potential [21] and the exchange–correlation energy of electrons is approximated by the local density approximation (LDA) [22]. The energy cutoff is set to be 500 eV and the surface Brillouin zone is sampled on a 7 × 7 regular mesh. The density of states is broadened with a 0.1 eV width. All atoms, including surface layers, are relaxed until the atomic forces are reduced below 0.02 eV $Å^{-1}$. For comparison, we carried out a test calculation on $H(LAO)_1(STO)_6$ (see below) with two bottom STO layers fixed to bulk positions, the results of which were found to be close to those with full relaxation. Artificial dipole layers are introduced in the vacuum space to eliminate the spurious dipole–dipole interactions between the repeated model slabs. The spin polarization is not taken into consideration because several test calculations reveal that the self-consistent spin density is negligible. (The initial spin moments are distributed around the H atom.)

As a model structure, we employ $(LAO)_n(STO)_6$ ($n = 1$, 2, 5, 7) which consists of n unit layers of LAO and six unit layers of STO. In [10], the STO layer was expanded up to 30 unit layers in order to study the long-range tail of the transferred electron. However, the charge-transfer mechanism and the amount of charge transfer do not depend significantly on the STO length, and we found that the computations with six layers of STO produce a reasonable distribution of the charge density. We consider the n-type interface formed by a layer sequence of $(\cdots$–(AlO_2)–(LaO)–(TiO_2)–(SrO)–$\cdots)$. The surface end of STO is terminated with an additional TiO_2 layer because the SrO termination slightly affects the charge distribution, particularly in the tail region. On the opposite side of the slab, the AlO_2 layer is exposed to the vacuum (see figure 1(a)). A vacuum space with a thickness of about 20 Å is inserted between neighboring slabs. The side view of the model system is shown in figure 1(a). The two-dimensional lattice parameters in the xy-plane are fixed to 3.8725 Å, the theoretical cell parameter of bulk STO. This reflects the experimental situation where LAO is grown on top of the thick STO substrate. In sections 3.1 and 3.2, we carry out extensive analysis on the adsorption of one H atom per (1×1) surface unit cell. The adsorption with lower H densities will be discussed in section 3.3.

3. Results

3.1. Adsorption energy of hydrogen

To study the hydrogen adsorption on the (1×1) surface of $(LAO)_n(STO)_6$, various adsorption sites are examined on the

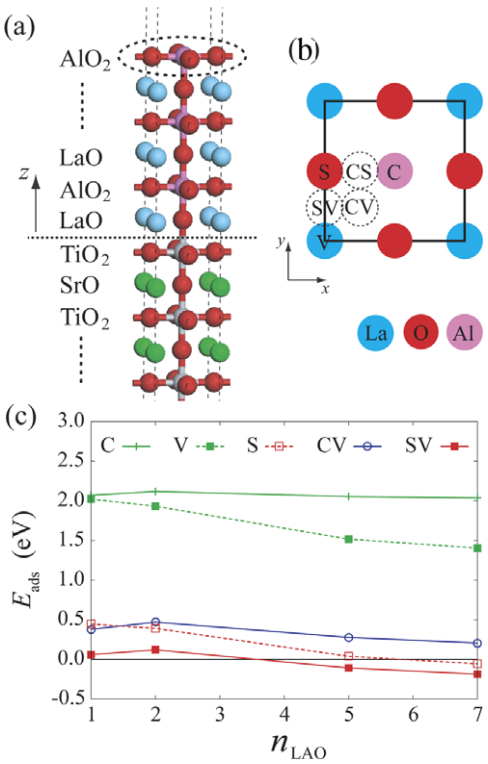

Figure 1. (a) The side view of a slab model system. The surface layer of AlO_2 is marked with a dashed oval. (b) The adsorption sites on the AlO_2 surface are marked in the top view. (c) The hydrogen adsorption energy (E_{ads}) for each adsorption site is shown as a function of LAO layers (n_{LAO}).

AlO_2 surface layer. In figure 1(b), symmetrically distinct adsorption sites are denoted; on top of Al at the center (C), on top of O at the side (S), above subsurface La at the vertex (V). In addition, positions between the high-symmetry sites are also considered (CS, CV, and SV). To compare the energetic stability, we define the adsorption energy (E_{ads}) as follows;

$$E_{ads} = E_{H/LAO/STO} - (E_{LAO/STO} + \mu_H) \qquad (1)$$

where $E_{H/LAO/STO}$ and $E_{LAO/STO}$ are the total energies of LAO/STO with and without the hydrogen adatom, respectively, and μ_H indicates the chemical potential of hydrogen. For convenience, μ_H is set to half of the total energy of the H_2 molecule calculated within the present computational scheme. Therefore, a negative sign in E_{ads} means that the dissociation of H_2 and adsorption on the specific site is an exothermic process at 0 K. The H atom can also bind to the surface through the dissociation of H_2O molecules, as shown in the following chemical reaction;

$$LAO/STO + \tfrac{1}{2}H_2O \rightarrow H/LAO/STO + \tfrac{1}{4}O_2. \qquad (2)$$

In this case, the exothermic condition requires E_{ads} to be lower than −1.45 eV.

Figure 1(c) shows E_{ads} for various adsorption sites with respect to the number of LAO unit layers (n_{LAO}). The CS site turns out to be unstable, as the H atom in that configuration relaxes to the S site. In figure 1(c), SV sites are most

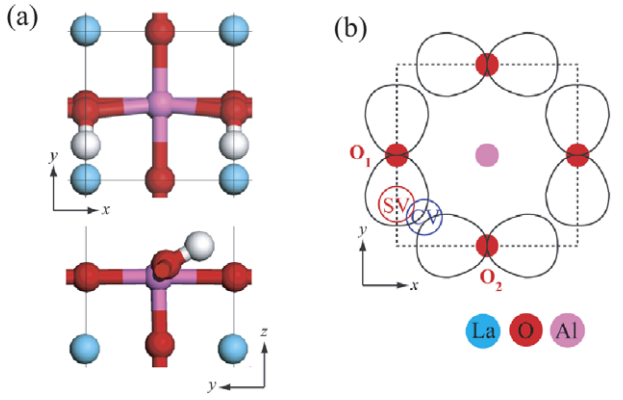

Figure 2. (a) Top and side views of the bonding geometry with hydrogen at the most stable SV site. (b) Schematic of orbital shapes in the surface band. O_1 designates the oxygen atom bonded to the H atom and O_2 is the other oxygen atom in the unit cell.

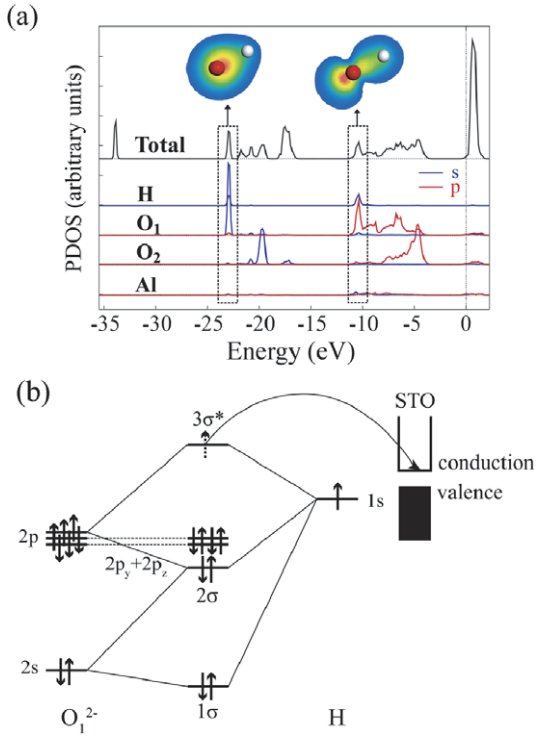

Figure 3. (a) Atom-resolved partial density of states (PDOS) for the top AlO_2 layer of $H(LAO)_7(STO)_6$. The Fermi level is set to zero. O_1 is the oxygen atom bound to the hydrogen. The isosurfaces in the inset show the charge distribution between O_1 and H atoms, summed over the dashed boxes. (b) Schematic diagram depicting the chemical bonding between O_1 and H atoms.

favored for all thicknesses of LAO, closely followed by the S site. Because of the large difference in electronegativity, the hydrogen prefers to form a bond with oxygen. The bonding geometry at the SV site does not vary significantly with the LAO thickness, and one typical case is presented in figure 2(a). It is seen that the H atom adsorbs at the oxygen site from the side with a bond length of 0.99 Å, rather than the on-top S site. (A similar adsorption configuration was found for the STO surface [23].) This can be understood from the orbital shape in the surface band. In [10], it was shown that the valence top of the LAO–STO heterostructure is mainly composed of O 2p orbitals lying in the surface plane, as schematically described in figure 2(b). In the case of the O_1 atom bonded to the H atom, this O 2p orbital is pointing to the y-direction. Therefore, the H atom is attracted to this direction to maximize the overlap integral between H 1s and O 2p orbitals, making the SV site most favorable. This is also confirmed from the analysis on the partial density of states (PDOS) below. Similarly, the CV site is locally stabilized near the V site where the overlap with the nearby O 2p orbitals is maximized (see figure 2(b)).

Another interesting feature in figure 1(c) is the dependence of E_{ads} on the thickness of LAO. For $(LAO)_1(STO)_6$ and $(LAO)_2(STO)_6$, the positive sign in E_{ads} indicates that virtually no hydrogen atom is stabilized on the top AlO_2 layer with respect to H_2. When n_{LAO} is greater than a certain critical value of three or four, however, E_{ads} on S and SV sites becomes negative. Similar tendencies of the stabilization are noticeable for every adsorption site except for the C site. This stronger adsorption with larger n_{LAO} can be rationalized by the electronegative nature of oxygen. When n_{LAO} is greater than three, electrons are transferred from LAO to STO [10]. This results in hole states distributed over the surface oxygen atoms. That is to say, surface oxygen atoms are in a more electron-deficient environment as the LAO stack becomes thicker. Therefore the H adatom, which is less electronegative than oxygen, can form a stronger chemical bonding by supplying electrons to the underlying O atoms.

To investigate the bonding character between the adatom and the surface oxygen, the electronic structures are further analyzed. Figure 3(a) shows the atom-projected PDOS in the top AlO_2 layer of $H(LAO)_7(STO)_6$. At the energies around −23 and −11 eV (marked by dashed boxes), the strong chemical bonding between H and O_1 can be noted. The charge distributions at these energies are shown in the upper part of the figure 3(a), which clearly shows that ss_σ and sp_σ bondings are formed. As a result, the 2p level of the O_1 atom is significantly lowered as compared to that of the O_2 atom which is not bonded to the H atom. Based on this analysis, the chemical bonding between O_1 and H atoms can be described pictorially in figure 3(b). This type of bonding orbital is typical in binuclear hydrogen compounds which include highly electronegative elements (e.g., HF) [24].

3.2. Band structures

In order to investigate how the electronic structures are affected by the H adsorption, we analyze the band structure in figure 4. In figures 4(a) and (b), the band structures of $(LAO)_1(STO)_6$ and $(LAO)_7(STO)_6$ without adatoms are shown, respectively. For $(LAO)_1(STO)_6$, the system is insulating with a well-defined energy gap. When the thickness of LAO exceeds the critical value of three layers, as in $(LAO)_7(STO)_6$, the LAO surface band at the M point rises above the conduction band of STO at the Γ point, triggering electron transfer from LAO to STO (see figure 4(b)). This generates hole states in the LAO surface and electron carriers in STO [10]. The amount of charge transfer per unit cell increases with n_{LAO}, and is

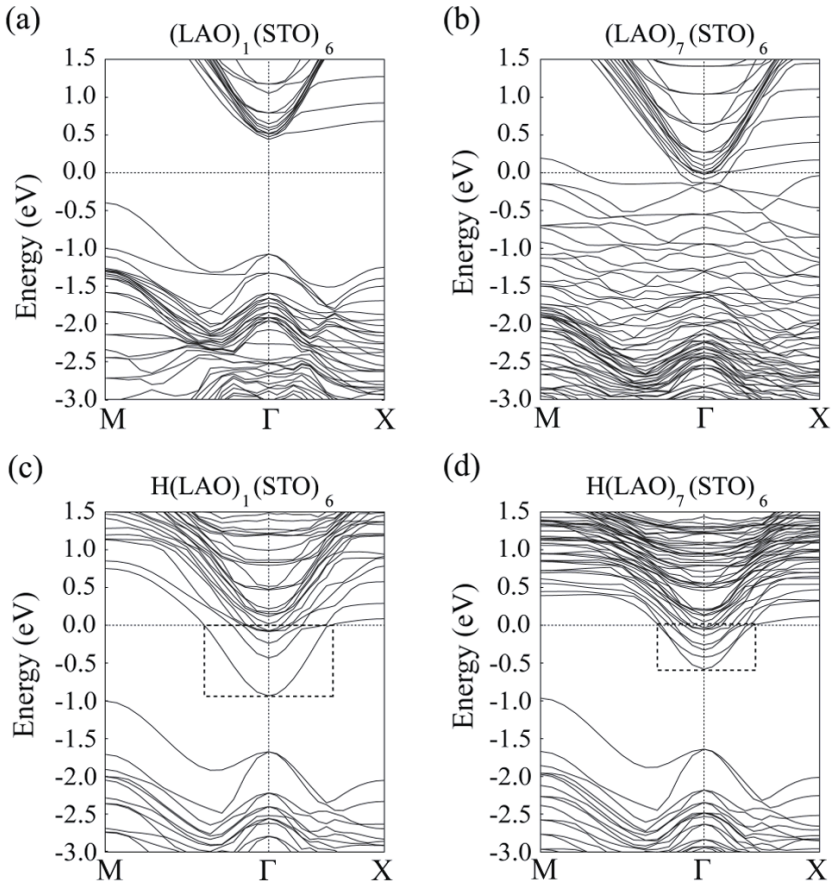

Figure 4. (a), (b) show the band structures of $(LAO)_1(STO)_6$ and $(LAO)_7(STO)_6$, and (c), (d) show the band structures of $H(LAO)_1(STO)_6$ and $H(LAO)_7(STO)_6$, respectively. The Fermi level is set to zero. When the H atom is adsorbed, one electron is transferred to the conduction-like bands, as shown by the dashed boxes in (c) and (d).

saturated at $0.5e$, at which point the potential divergence is completely eliminated.

The electronic structures change significantly with the H adsorption. Figures 4(c) and (d) show the band structure when one H atom is attached to the most stable SV site of $(LAO)_1(STO)_6$ and $(LAO)_7(STO)_6$, respectively. In both figures, it is found that one electron occupies the conduction-like bands (see dashed boxes). For $H(LAO)_1(STO)_6$, this state is mainly Ti 3d orbitals slightly mixed with La orbitals, similarly to that in $(LAO)_7(STO)_6$. Therefore, one electron is transferred from the adsorbed hydrogen to the STO layer. The charge-transfer mechanism is schematically depicted in figure 3(b). The bonding states from the hybridization of O and H orbitals are far below the Fermi level while the anti-bonding states lie much higher than the Fermi level due to the strong σ-bonding nature. An electron occupying this state then drops to the conduction band of STO, which is lower in energy. It is also noted, in figures 4(b) and (d), that the electronic states between -1.7 and 0 eV for $(LAO)_7(STO)_6$ disappear upon H adsorption. From the analysis on the layer-projected density of states (LDOS), it is found that these energy bands are mostly contributed by the valence states of LAO, not just the surface layer but the whole LAO stack. As will be shown below, these states are the result of the increasing potential inside LAO. The H adsorption reverses the sign of the potential slope, and, therefore, the electronic bands in LAO shift down significantly. In passing, we also performed calculations on $H(LAO)_1(STO)_6$ with the H atom adsorbed at S and CV sites, for which E_{ads}s are similar to that for the SV site, and it was found that the band structures are similar to that for the SV site in figure 4(c).

In $H(LAO)_7(STO)_6$, the band structure in figure 4(d) indicates that one electron occupies the conduction-like bands, as in $H(LAO)_1(STO)_6$. However, the charge distribution of these states is significantly different; figure 5 shows the xy-averaged charge density ($\bar{\rho}(z)$) contributed by the states inside the dashed box of figure 4(d). Here $\bar{\rho}(z)$ is calculated from the charge density $\rho(x, y, z)$ by the following equation:

$$\bar{\rho}(z) = \frac{1}{A}\int_A \rho(x, y, z)\,\mathrm{d}x\,\mathrm{d}y, \tag{3}$$

where A is the unit cell area in xy-dimensions. From the figure, it is seen that the charges are split between STO and LAO. By integrating the charge density in each domain, we find that $0.366e$ and $0.634e$ are distributed in LAO and STO layers, respectively. The transferred charges in STO are composed of d_{xy} orbitals at Ti sites near the interface while those in the LAO layer are mostly of La 5d and Al 3s characters. The charge splitting can be understood from the electrostatic boundary conditions; as one electron is transferred from LAO to STO,

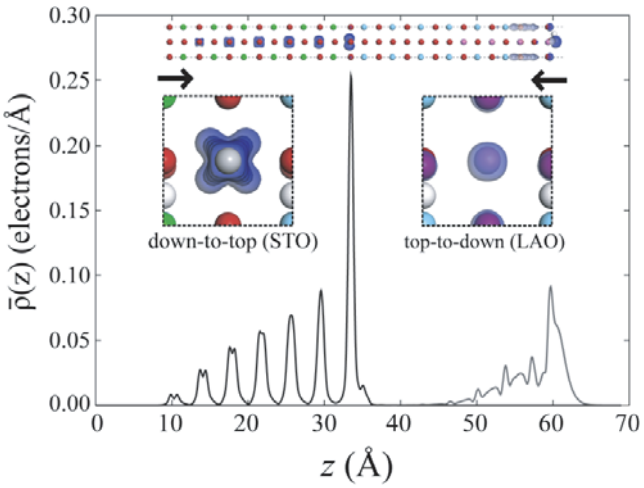

Figure 5. The xy-averaged charge density ($\bar{\rho}(z)$) of $H(LAO)_7(STO)_6$ contributed by the states in the dashed boxes in figure 4(d). The inset figures show the charge distribution from the side, top, and bottom viewpoints, respectively.

Table 1. The fraction of electronic charges transferred from one H atom to LAO and STO (ρ_{LAO} and ρ_{STO}, respectively) is shown with respect to the LAO layers (n_{LAO}).

n_{LAO}	1	2	5	7
ρ_{LAO} (e)	0.000	0.093	0.304	0.366
ρ_{STO} (e)	0.999	0.907	0.696	0.634

the electrostatic potential in LAO decreases because more than $0.5e$, a condition for the flat potential, is added at the interface. This lowers the conduction band of the LAO surface, which mainly consists of states at cation sites. The analysis for other thicknesses of LAO is presented in table 1. It is found that the charges in LAO (ρ_{LAO}) increase while those in STO (ρ_{STO}) decrease with n_{LAO}. Since the potential divergence can be avoided by a charge transfer of $0.5e$, ρ_{LAO} and ρ_{STO} should eventually converge to $0.5e$ in the limit of $n_{LAO} = \infty$.

To further understand how the charge transfer affects the potential divergence inherent in the polar–nonpolar interface, we examine the local electrostatic potential in figure 6(a). The thick solid line shows the macroscopically averaged potential ($\bar{\bar{V}}(z)$) that is calculated by the following equation:

$$\bar{\bar{V}}(z) = \frac{1}{l_1 l_2} \int_{z-l_2/2}^{z+l_2/2} \mathrm{d}z' \int_{z'-l_1/2}^{z'+l_1/2} \bar{V}(z'')\,\mathrm{d}z'' \qquad (4)$$

where l_1 and l_2 are the lattice parameters of LAO and STO, respectively, and $\bar{V}(z)$ is the xy-average of the local potential computed using equation (3) (the thin solid line). For comparison, the macroscopic potential for $(LAO)_7(STO)_6$ is shown as a dashed line, which shows that the potential increases along the z-direction. In contrast, the potential in $H(LAO)_7(STO)_6$ decreases towards the LAO surface. This is because $0.634e$ is transferred from LAO to STO. As mentioned above, the potential flattens only when $0.5e$ is transferred. When the charge transfer is greater than this value, the potential bends downwards. Figure 6(b) shows the LDOS for

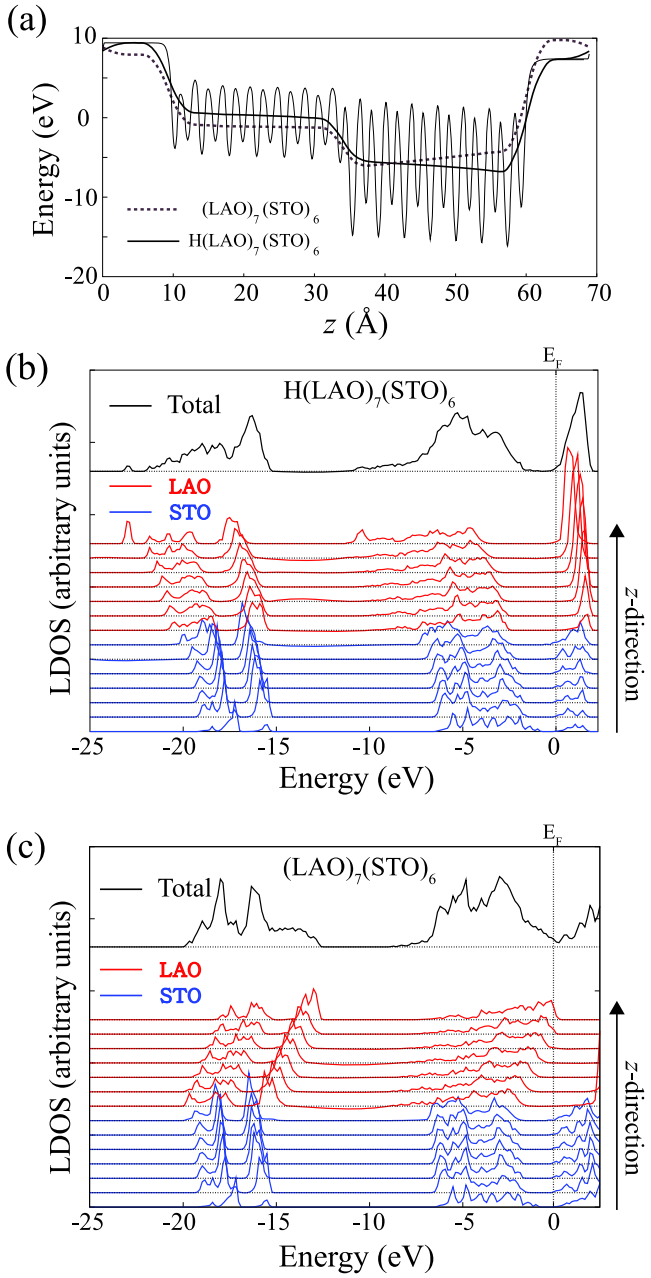

Figure 6. (a) The xy-averaged local potential (solid line) and macroscopically averaged local potential (thick solid line) of $H(LAO)_7(STO)_6$. The dashed line stands for the macroscopically averaged local potential of $(LAO)_7(STO)_6$. (b) Layer-projected density of states (LDOS) of $H(LAO)_7(STO)_6$. Blue and red lines are for STO and LAO, respectively. The Fermi level (E_F) is set to zero. Note that each LDOS curve consists of the whole compositional unit, i.e., ($LaO + AlO_2$) or ($SrO + TiO_2$). (c) LDOS for $(LAO)_7(STO)_6$ plotted in the same way as in (b).

$H(LAO)_7(STO)_6$. From the LDOS near the Fermi level, it is confirmed that the double charge layer in figure 5 originates from the LAO surface and the interfacial STO layer. In addition, the local bands are bending, as can be confirmed by the conduction and valence edges. This downward band bending is consistent with the macroscopically averaged local potential in figure 6(a). In figure 6(b), it is also noted that the O–H bonding formed around −23 and −11 eV (see figure 3(a))

is confined within the surface layer. For comparison, LDOS for $(LAO)_7(STO)_6$ is presented in figure 6(c) and it is seen that the band edges in LAO rise along the z-direction, which is consistent with the macroscopic potential in figure 6(a).

For comparison, we also performed calculations with fluorine (F) adatoms instead of hydrogen. It is found that the adsorption at the C site (i.e., on the central Al atom) is most favored because of the strong electronegativity of F. In contrast to the H adsorption, the conduction bands are not pulled down by the F adsorption, and the charge-transfer mechanism inferred from the band structure is rather similar to that of the reference system without adatoms. A strong Al–F bond is formed, but unlike the O–H case, there is no electron in Al to occupy the anti-bonding state and, therefore, charge transfer does not occur.

3.3. Dependence on surface density of hydrogen

So far it has been assumed that one H atom is attached to every (1×1) unit cell. In order to study the dependence of E_{ads} on the surface density of hydrogen, we consider lower H densities by introducing one H atom to every (2×1) or (2×2) surface unit cell. By comparing the adsorption energies for low-energy adsorption configurations at SV, S, and CV sites, it is confirmed that the SV sites are always favored. The analysis on the charge distribution indicates that the charge transfer in these lower H densities occurs from the H atom to the STO slab regardless of LAO thickness. This is in contrast to the adsorption on the (1×1) unit cell, wherein the charge fraction transferred to STO is reduced as the LAO thickness is increased. This is because the local potential does not decrease for the lower H densities. For example, in the case of the (2×1) overlayer, half an electron is transferred for every (1×1) unit cell, which results in the flat band inside LAO, as can be confirmed from the local potential in figure 7(a) (see the dashed line). For H adsorption on every (2×2) unit cell, the charge transfer of $0.25e$ per unit cell is not enough to eliminate the Coulombic instability, and the electrostatic potential still rises, as shown by the dotted line in figure 7(a). These results also imply that if two H atoms are attached to each (1×1) unit cell, the potential will decrease more rapidly than for the (1×1) overlayer.

In figure 7(b), E_{ads} is compared between $(LAO)_1(STO)_6$ and $(LAO)_5(STO)_6$ with (1×1), (2×1), and (2×2) H overlayers. It is found that E_{ads} is greatly reduced as the H density is lowered. This is due to the repulsive interaction between parallel electric dipoles that originate from the charge transfer between H and the underlying LAO–STO heterostructure. As the thickness of LAO increases, the magnitude of the dipole moment also increases, which explains the more pronounced dependence on the H density in figure 7(b). One intriguing feature in figure 7(b) is that E_{ads} is much lower for the thicker LAO layer with low H densities. This is because the energy gain from mitigating the Coulombic divergence increases with the LAO thickness. In the case of the (1×1) H overlayer, the degree of instability is similar to the unhydrogenated surface, and E_{ads} weakly depends on n_{LAO}.

The foregoing analysis bears an important implication for the hydrogenation behavior of LAO–STO heterostructures. In

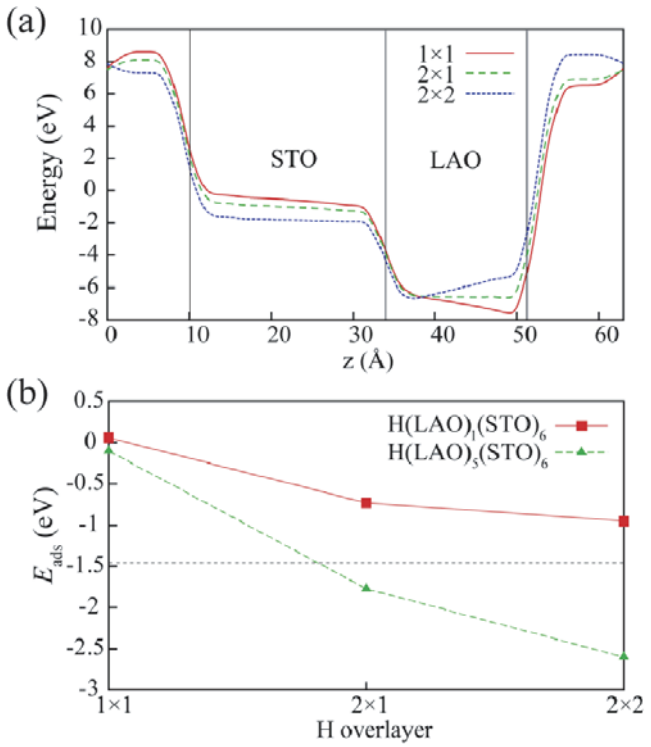

Figure 7. (a) The macroscopically averaged potentials for $H(LAO)_5(STO)_6$ with (1×1), (2×1), and (2×2) H overlayers. Different potential slopes are noticeable inside LAO. (b) The adsorption energies (E_{ads}) for $(LAO)_1(STO)_6$ and $(LAO)_5(STO)_6$ with different H overlayers. The dashed line at -1.45 eV indicates the chemical potential of hydrogen when a dissociative reaction occurs from the H_2O molecules to produce O_2 molecules (see text).

equation (1), the chemical potential of hydrogen was set to the half of the total energy of the H_2 molecule. If one takes into account the overbinding of the LDA method [3], as well as the decrease of μ_H at ambient conditions [25], the dissociative adsorption of H_2 would be exothermic when E_{ads} is less than ~ -1.0 eV. If humidity becomes the hydrogen source instead of H_2 gas, μ_H at 0 K corresponds to -1.45 eV (see section 3.1), which is indicated by a dashed line in figure 7(b). Therefore, the present computational results suggest that when the LAO layer is thin, as in $(LAO)_1(STO)_6$, the hydrogenation of the LAO surface would not be favorable whether the source is H_2 or H_2O molecules. Only when LAO is thicker than some critical value (for example, five layers) will the hydrogenated surface be stabilized with a finite areal density of hydrogen. In [26], the metallic conductivity of LAO–STO heterointerfaces was observed for an LAO thickness greater than three layers. The variation of E_{ads} with respect to the LAO thickness found in the present work, therefore, may provide an alternative explanation for this phenomenon apart from the intrinsic origin [10, 11].

4. Conclusions

In summary, we have carried out first-principles studies on the hydrogenation of the AlO_2 surface of LAO–STO heterostructures with an n-type interface. The adsorption on

the surface O atom was always favored and the adsorption energy for a given H density reduces with increasing LAO thickness. The adsorbed H atom was found to donate electrons to the conduction band of STO, which results in the metallic conductivity of STO. Concurrently, the charge transfer from H to STO significantly alters the electrostatic boundary condition and the Coulombic divergence inside the LAO completely disappears when one H atom is adsorbed every (2×1) surface unit cell. Our results also indicate that H_2 or H_2O molecules exothermically dissociate and adsorb on the surface when the LAO layer is thick enough, suggesting that H adsorption may play a role in the conducting properties of LAO–STO heterostructures observed in experiments. A controlled experiment with different humidity or H_2 partial pressure could verify the hydrogen-induced carrier generation mechanism identified in this study. The present work also suggests that the chemical activity of the surface of LAO–STO heterointerfaces can be tuned by controlling the thickness of LAO. This could be exploited in its application to hydrogen sensors or hydrogen storage materials.

Acknowledgments

This work was supported by the Quantum Metamaterials Research Center (Grant No. R11-2008-053-03001-0) and the Basic Science Research Program (2009-0092809) through the National Research Foundation of Korea. The computations were carried out at KISTI Supercomputing Center (KSC-2009-S03-0008).

References

[1] Tasker P W 1979 *J. Phys. C: Solid State Phys.* **12** 4977
[2] Noguera C 2000 *J. Phys.: Condens. Matter* **12** R367
[3] Lanier C H, Rondinelli J M, Deng B, Kilaas R, Poeppelmeier K R and Marks L D 2007 *Phys. Rev. Lett.* **98** 086102
[4] Nakagawa N, Hwang H Y and Muller D A 2006 *Nat. Mater.* **5** 204
[5] Ohtomo A and Hwang H Y 2004 *Nature* **427** 423
[6] Popovic Z S, Satpathy S and Martin R M 2008 *Phys. Rev. Lett.* **101** 256801
[7] Lee J and Demkov A A 2008 *Phys. Rev.* B **78** 193104
[8] Pentcheva R and Pickett W E 2006 *Phys. Rev.* B **74** 035112
[9] Janicka K, Velev J P and Tsymbal R Y 2009 *Phys. Rev. Lett.* **102** 106803
[10] Son W, Cho E, Lee B, Lee J and Han S 2009 *Phys. Rev.* B **79** 245411
[11] Ishibashi S and Terakura K 2008 *J. Phys. Soc. Japan* **77** 104706
[12] Huijben M, Brinkman A, Koster G, Rijnders G, Hilgenkamp H and Blank D H A 2009 *Adv. Mater.* **21** 1665
[13] Pauli S A and Willmott P R 2000 *J. Phys.: Condens. Matter* **20** 264012
[14] Willmott P R, Pauli S A, Herger R, Schlepütz C M, Martoccia D, Patterson B D, Delley B, Clarke R, Kumah D, Cionca C and Yacoby Y 2007 *Phys. Rev. Lett.* **99** 155502
[15] Cen C, Thiel S, Hammerl G, Schneider C W, Andersen K E, Hellberg C S, Mannhart J and Levy J 2008 *Nat. Mater.* **7** 298
[16] Li Y, Phattalung S N, Limpijumnong S and Yu J 2009 arXiv:0912.4805
[17] Goniakowski R J, Finocchi F and Noguera C 2008 *Rep. Prog. Phys.* **71** 016501 and references therein
[18] Wang Y, Meyer B, Yin X, Kunat M, Langenberg D, Traeger F, Birkner A and Wöll Ch 2005 *Phys. Rev. Lett.* **95** 266104
[19] Rocker G and Göpel W 1986 *Surf. Sci.* **175** L675
[20] Kresse G and Hafner J 1993 *Phys. Rev.* B **47** 558
[21] Blöchl P E 1994 *Phys. Rev.* B **50** 17953
[22] Ceperley D M and Alder B J 1980 *Phys. Rev. Lett.* **45** 566
[23] Lin F, Wang S, Zheng F, Zhou G, Wu J, Gu B-L and Duan W 2009 *Phys. Rev.* B **79** 035311
[24] Jean Y and Volatron F 1993 *An Introduction to Molecular Orbitals* (New York: Oxford University Press)
[25] Chase M W Jr, Davies C A, Downey J R Jr, Frurip D J, McDonald R A and Syverud A N 1985 JANAF thermochemical tables third edition *J. Phys. Chem. Ref. Data, Suppl.* **14** 1
[26] Thiel S, Hammerl G, Schmehl A, Schneider C W and Mannhart J 2006 *Science* **313** 1942